Biosafety and Efficacy Evaluation of a Biodegradable Magnesium based Drug-eluting Stent in Porcine Coronary Artery

Jinzhou Zhu
Department of Cardiology, RuiJin Hospital, School of Medicine, Shanghai Jiao Tong University

Xiyuan Zhang
National Engineering Research Center of Light Alloy Net Forming and Key State Laboratory of Metal Matrix Composites, Shanghai Jiao Tong University

Jialin Niu
National Engineering Research Center of Light Alloy Net Forming and Key State Laboratory of Metal Matrix Composites, Shanghai Jiao Tong University

Yongjuan Shi
National Engineering Research Center of Light Alloy Net Forming and Key State Laboratory of Metal Matrix Composites, Shanghai Jiao Tong University

Zhengbin Zhu
Department of Cardiology, RuiJin Hospital, School of Medicine, Shanghai Jiao Tong University

Daopeng Dai
Department of Cardiology, RuiJin Hospital, School of Medicine, Shanghai Jiao Tong University

Chenxin Chen
National Engineering Research Center of Light Alloy Net Forming and Key State Laboratory of Metal Matrix Composites, Shanghai Jiao Tong University

Jia Pei
National Engineering Research Center of Light Alloy Net Forming and Key State Laboratory of Metal Matrix Composites, Shanghai Jiao Tong University

Guangyin Yuan
National Engineering Research Center of Light Alloy Net Forming and Key State Laboratory of Metal Matrix Composites, Shanghai Jiao Tong University

Ruiyan Zhang (rjzhangruiyan@aliyun.com)
Department of Cardiology, RuiJin Hospital, School of Medicine, Shanghai Jiao Tong University

---

Research Article

Keywords: Coronary artery disease, Bioresorbable stent, magnesium alloy

Posted Date: November 25th, 2020

DOI: https://doi.org/10.21203/rs.3.rs-110813/v1

Version of Record: A version of this preprint was published at Scientific Reports on April 1st, 2021. See the published version at https://doi.org/10.1038/s41598-021-86803-0.

Biosafety and Efficacy Evaluation of a Biodegradable Magnesium based Drug-eluting Stent in Porcine Coronary Artery

Jinzhou Zhu[1, #], Xiyuan Zhang[2,#], Jialin Niu[2,#], Yongjuan Shi[2], Zhengbin Zhu[1], Daopeng Dai[1], Chenxin Chen[2], Jia Pei[2], Guangyin Yuan[2,*], Ruiyan Zhang[1,*]

[1] Department of Cardiology, RuiJin Hospital, School of Medicine, Shanghai Jiao Tong University, Shanghai, 20025, P.R. China

[2] National Engineering Research Center of Light Alloy Net Forming and Key State Laboratory of Metal Matrix Composites, Shanghai Jiao Tong University，Shanghai, 200240, P.R. China

[#] These authors contributed equally to this work.

[*]Correspondence to: Guangyin Yuan, Email: gyyuan@sjtu.edu.cn; Ruiyan Zhang, Email: rjzhangruiyan@aliyun.com.

Abstract

Although drug-eluting stent (DES) has become the standard for percutaneous coronary interventions (PCI) based revascularization, stent thrombosis has emerged as a major cause of death and morbidity for those clinical commonly used permanent stents. Drug-eluting bioresorbable stent (BRS) was thus developed as an alternative to DES, which can be completely absorbed after its therapeutic period. Among them, magnesium (Mg) based BRS has attracted great attention due to its suitable mechanical properties, innovative chemical features and well-proven biocompatibility. In the present work, a Mg–Nd–Zn-Zr (JDBM) based drug-eluting BRS loaded with rapamycin was prepared, and its biosafety and efficacy for coronary artery stenosis were evaluated via in vitro and in vivo experiments. The smooth muscle cells adhesion of PDLLA/RAPA coated alloy and the rapamycin pharmacokinetics of JDBM BRS were first

assessed in vitro. JDBM BRS and commercial DES Firehawk were then implanted in the coronary arteries of a porcine model. Neointimal hyperplasia was evaluated at 30, 90, and 180 days, and re-endothelialization was evaluated at 30 days. Furthermore, Micro-CT and optical coherence tomography (OCT) analysis were performed to evaluate the technical feasibility and biocompatibility of JDBM alloy based drug-eluting BRS in vivo. The results showed the inhibition ability of PDLLA/RAPA coated JDBM to smooth muscle cells adhesion and moderate drug release rate of JDBM BRS, demonstrating good anti-restenosis ability in vitro. In vivo, low local and systemic risks of JDBM alloy based BRS was demonstrated in the porcine model. We also showed that this novel BRS was associated with a comparable efficacy profile and high anti-restenosis performance. These findings may confer long term advantages for the use of this BRS over a traditional DES.

Keywords: Coronary artery disease, Bioresorbable stent, magnesium alloy

1. Background

Strategies for the treatment of coronary artery disease (CAD) have made great progress in the past decades. The first performed balloon angioplasty in 1977 changed the landscape of CAD treatment. Bare metal stent (BMS) heralded the second revolution as a means to conquer the drawbacks of balloon angioplasty including acute vessel recoil, late constrictive remodeling, and diffuse restenosis. Drug-eluting stent (DES), the third revolution in interventional cardiology, has now become the gold standard in percutaneous myocardial revascularization, as it has been demonstrated to reduce the in-stent restenosis rate and incidences of major cardiac adverse events (MACE) by inhibiting the proliferation of smooth muscle cells compared with BMS [1, 2]. However, a few concerns remain regarding the use of DES, mainly due to its permanent rigid

constraint to vessels and consequences like late stent thrombosis (ST) [3-5]. In addition, other issues were identified including reduction of side-branch flow, abnormal vasomotion because of the permanent metallic caging, and interference with the future surgical revascularization [6-8].

Drug-eluting bioresorbable stent (BRS) was thus developed as an alternative to DES. It could provide temporary support to the vessel wall, and be fully resorbed after the vessel restoring its physiological function [9-13]. The first generation of poly-L-lactic acid (PLLA) based stent (Absorb^{TM}, Abbott Vascular) showed promising results at 1 year post operation. However, it had several limitations including increased strut thickness and crossing profile, relatively low resistance to overexpansion, which originates from its poor mechanical properties. These weaknesses caused an increased risk of ST and target vessel myocardial infarction in the long term reports, and consequently, Abbott Vascular has to halt recently. Moreover, PLLA based BRS lacks radiopacity, resulting in a more frequent need for intravascular imaging modalities to achieve reasonable device deployment.

The new generation of magnesium (Mg) based BRS has attracted great attention recently. It has suitable mechanical properties and radiopacity so that can overcome the drawbacks of PLLA polymer stents. At the same time, by alloy design and adopting bioactive coating, the in vivo degradation process of Mg based BRS could be regulated, and the degradation products, being mainly Mg ions, have been proved to have good biocompatibility. Historically biodegradable Mg based materials have been used in therapeutic medicine in different areas including wound closure, dental procedures and cardiovascular surgery, etc. The biocompatibility of Mg based BRS devices in vascular tissue has been demonstrated in porcine coronary arteries with rapid endothelialization and low inflammatory response [14]. In contrast with PLLA BRS, Mg shows better radial force,

pushability and trackability. However, the primary disadvantage of Mg based BRS is its high corrosion rates with complete biodegradation within 3 months, while ideal BRS should have adequate radial support for a period of about 6 months to prevent recoil and constrictive remodeling.

Recently, a new type of patented Mg–Nd–Zn-Zr alloy (Jiao Da BioMg, denoted as JDBM) has been developed in Shanghai Jiao Tong University [15, 16]. In this Bio-Mg alloy series, Nd was selected as the main alloying element, accompanied by the microalloyed Zn and Zr. Nd is one of light rare earth elements showing little cytotoxicity, the addition of which has already exhibited significant strengthening effect in Mg-Nd binary alloys [17], and could greatly slow down galvanic corrosion between Mg matrix and second phases [15, 18]. As a result, the novel JDBM material possesses excellent mechanical properties, good biocompatibility. a slower corrosion rate and more uniform degradation behavior over many commercial available Mg alloys, such as AZ31 and WE43 [16].

Aiming to further reduce the degradation rate of JDBM alloy and restore the physiological function of vessels, in the present study, we designed one type of drug coating-PDLLA/rapamycin (denoted as PDLLA/RAPA), and prepared it on JDBM alloy disk samples as well as stents successfully. The inhibition effects on smooth muscle cells and pharmacokinetics were studied in vitro, and the in vivo biosafety and efficacy were evaluated using a porcine coronary arteries model.

2. Methods

2.1 Materials and samples preparation

The composition and preparation process of JDBM alloy can be found in Ref. [19]. Disk samples

of Ø15×3 mm were cut from JDBM extruded bar for in vitro cell adhesion experiment. After being ground up to 3000 grit with SiC paper, the samples were immersed in HF to form MgF_2 film for lower degradation of JDBM, and then the PDLLA/RAPA coating was prepared on these disk samples using the same method in Ref. [20]. For stent preparation, JDBM mini-tube with an outer diameter of 3 mm and the wall thickness of 0.18 mm was prepared, and the stents were laser-carved from the mini-tube in MicroPort Medical Co., Ltd (Shanghai, China). The detailed process can be found in Ref. [21]. After electrochemical polishing, the stents were immersed in HF as mentioned above, and then the PDLLA/RAPA coating was prepared on these stents using the same method in Ref. [22]. The stents finishing preparation were denoted as JDBM BRS. As a control, the same structured 316 L SS stents loaded with PDLLA/RAPA coating were also prepared with the same method (SS BRS).

2.2 In vitro cell adhesion

Rat thoracic aorta smooth muscle cells line (A7r5) purchased from Cell Bank (Chinese Academy of Sciences, China) was selected to evaluate the cell adhesion status on PDLLA/RAPA coated JDBM. The cells were cultured in Dulbecco's Modified Eagle Medium (DMEM, Gibco, CA, USA) supplemented with 1% streptomycin/penicillin and 10% fetal bovine serum (FBS, Gibco, CA, USA) in a cell incubator with 37 °C humidified atmosphere containing 5% CO_2.

To study the effects of the coating on A7r5 cells, we prepared three types of disk samples, including PDLLA/RAPA coated JDBM (PDLLA/RAPA), PDLLA coated JDBM (PDLLA), and JDBM only immersed in HF without any polymer coating (HF-JDBM) disk samples. These samples were put in 24-well plates, and every well was added with 1ml 10000/ml cell suspension. The samples and cell suspension were co-incubated for one and three days, then the samples were

cleaned twice using PBS, and stained with 200μL calcein acetoxymethyl ester (Calcein-AM, Sigma, MO, USA) every well. Fifteen minutes later, the samples were cleaned with PBS again and then transferred onto slides. The morphology and quantity of cells were recorded by the inverted fluorescence microscopy (IX 71, Olympus, Japan) and analyzed by Image J software (NIH, MD, USA). A negative control group (NC) that cells were incubated in the blank well was also set.

2.3 In vitro pharmacokinetics

2.3.1 The standard curve of rapamycin

The standard curve of rapamycin should be measured to calibrate the drug release. 100 μg/mL liquid was prepared by dissolving 10 mg rapamycin with acetonitrile. Then the liquid was diluted to rapamycin standard solution with concentration of 50 μg/mL, 25 μg/mL, 12.5 μg/mL, 5 μg/mL, 2.5 μg/mL, 1 μg/mL, 0.5 μg/mL, 0.1 μg/mL respectively. The absorbance of rapamycin in gradient standard solution was measured by UV/Vis spectrophotometer (Thermo Spectronic Genesys 10, MA, USA). Finally, the standard curve of rapamycin was obtained by fitting the correlation between absorbance and concentration.

2.3.2 Rapamycin pharmacokinetics

To understand the pharmacokinetics of the real stents made by PDLLA/RAPA coated JDBM, the JDBM BRS we prepared was immersed in PBST (PBS containing 0.5 v/v% Tween 20) and then put in a shaker with the speed of 80 r/min at 37℃. At regular intervals, 2-5ml PBST was collected and replaced by the same volume of fresh PBST. After centrifuging the collected PBST at the speed of 13000 r/min, the supernate was collected to measure the absorbance by UV/Vis spectrophotometer (Thermo Spectronic Genesys 10, MA, USA). Drug concentration and accumulative release were calculated according to the standard curve of rapamycin. Then the

rapamycin pharmacokinetics curves were drawn and analyzed. The pharmacokinetics curve of SS BRS was tested as a control so as to reveal the impacts of JDBM degradation on drug release.

2.4 Porcine study

Animal experiments were conducted according to the standard protocols, animal welfare regulations, and the institutional guidelines of Shanghai Jiao Tong University School of Medicine and the Regulations for Practice of Experimental Animals (issued by Scientific and Technical Committee, PR China, 1988). All the procedures described were performed with the authorization of the Animal Use and Care Committee of Shanghai Jiao Tong University School of Medicine (approval number: SYKX-2008-0050).

Chinese domestic porcine obtained from Shanghai Agricultural College (Shanghai, China) with body weight between 55 and 90 kg were fed with normal laboratory chow diet for 7 days. The JDBM BRS and the control stent (Firehawk^{TM}, MicroPort Medical, Shanghai, China) were then implanted into coronary arteries under digital subtraction angiography (INNOVA2100, GE, USA) and followed for 30, 90, and 180 days. Briefly, arterial access was achieved by surgical exposure of the right common iliac artery with a 20 G puncture needle (Terumo, Tokyo, Japan). Coronary arterial angiography was then performed after intra-arterial administration of heparin (100 IU/kg), and the diameter of the coronary artery was measured with quantitative coronary angiographic analysis (QCA). Stents were implanted mainly in two major branches of the coronary artery: the left anterior descending and the right coronary artery. The balloon was inflated to 12 atm with the stent vessel ratio of 1.1:1. The arteriotomy and dermal layers were sutured after the catheter, wire, and sheath removed. The stenting procedure was always performed by the same investigators. Three days before the procedure and throughout the following period, all animals orally received

100 mg Aspirin and 75 mg Clopidogrel daily.

2.5 Quantitative coronary angiography

Angiography was performed before and after interventions and at 30, 90, and 180 days angiographic follow-up using identical projections and analyses. Offline quantitative measurements of the operation were performed with a computerized edge-detection quantitative coronary angiographic analysis software QAngio XA 7.2 (Medis Medical Imaging System BV, Leiden, the Netherlands) by an observer blinded to the study. After calibration with the outer diameter of the contrast-filled catheter, the minimum lumen diameter in different groups was determined in the proper frame.

2.6 Optical coherence tomography (OCT) analysis

Optical coherence tomography (OCT) was performed at 180 day follow-up using the OCT imaging system C7-XR with a catheter diameter of 2.7F (Light Lab Imaging, St. Paul, MN, USA) in experimental animals. The entire length of the stent was imaged with an automatic pullback device acquired at 20 mm/s. To clear away blood from the imaging site, a contrast solution was infused into the coronary artery during the retracement. All OCT frames were digitally stored and cross-sectional OCT images were analyzed at 0.2 mm intervals (every frame) using validated software (Light Lab Imaging, St. Paul, MN, USA) based on expert consensus. OCT parameters were calculated and defined as follows: Neointimal thickness was measured as the perpendicular distance between the endoluminal surfaces and the stent strut. The absence of definite neointima over the stent strut was defined as an uncovered stent strut. Thrombus was defined as an irregular mass protruding into the lumen or intraluminal mass with signal-free shadowing unconnected to the luminal surface.

2.7 Micro-CT analysis

Micro-CT scanning was performed to acquire a whole set of raw data along the entire length of the stent sample in the present study (SkyScan 1176, Kontich, Belgium). The long axis was aligned perpendicularly to the axis of the X-ray beam. Constant settings for X-ray energy and image capture were maintained. The obtained projection images were processed with the NRecon image reconstruction software using a convolution and back projection algorithm to produce a stack of 8-bit BMP images, each one of them representing a slice of the sample. Finally, a full three-dimensional (3D) model and animation were generated for visualization of the scaffold.

2.8 Scanning electronic microscopy (SEM) observation

Animals were sacrificed at 30, 90, and 180 days post implantation and the stented arterial segments were examined en face by SEM for analysis of potential stent and late stent thrombosis incidence. The stented arterial was first flushed with PBS for 1 min followed by a gentle flush with 10% buffered formalin for 30 s. Samples were further fixed with 2.5% glutaraldehyde in 0.1M sodium cacodylate buffer overnight and washed thrice with cacodylate buffer. Post-fixation was completed with 1% osmium tetroxide in 0.1 M cacodylate buffer, then serially dehydration with ethanol (30, 50, 70, 90, 95, and 100%), and critical point drying with CO_2. After drying, samples were gold sputtered and visualized under SEM (Quanta 250, FEI, OR, USA). The images of the cross sections of the stented arteries were analyzed. Regions of interest were imaged at incremental magnifications.

2.9 Histological analysis

The animals were sacrificed by potassium chloride injection and the stented arterial segments, obtained at 30, 90, and 180 days, were processed for histological examination. Samples were

dehydrated in a graded series of ethanol and embedded in methylmethacrylate plastic. After polymerization, the center section of each stent was cut on a rotary microtome (EXAKT, Norderstedt, Germany) into 10 μm thick sections and stained with Masson. An experienced pathologist, who was blinded to the groups, performed all histological analysis with the method reported previously [23].

2.10 Statistics

Continuous variables were presented as mean ± standard deviation (S.D.), and categorical variables were presented as counts and percentages. Statistically significant differences over time in the same treatment group, or among different treatment groups at a single time point were determined by one-way analysis of variance (ANOVA), followed by two-tailed Student's t-tests. Statistical analyses were performed with SPSS 17.0 (IBM, Armonk, NY, USA). Statistical significance was assumed for P values < 0.05.

3. Results

3.1 In vitro cell adhesion

The adhesion states of smooth muscle cells on PDLLA/RAPA-coated JDBM, PDLLA coated JDBM, HF-JDBM samples and Negative control (NC) were shown in Fig. 1, and the cell densities were counted as shown in Fig. 2. After incubated for 1 day, there was no obvious difference in cell density among the four groups, and only PDLLA/RAPA group showed a slightly lower cell density. However, after incubated for 3 days, four groups displayed diversity. The smooth muscle cell density increased 4 and 2.5 times in NC and PDLLA group respectively, while there had no evident change in HF-JDBM group. Conversely, the cell density decreased in PDLLA/RAPA group. The results of cell adhesion indicated that by loading rapamycin (RAPA), PDLLA/RAPA

coating on JDBM could inhibit the proliferation of smooth muscle cells effectively. This was realized by controlling the rapamycin release. The specific research on drug release will be shown subsequently.

3.2 In vitro pharmacokinetics

The pharmacokinetics curves of JDBM BRS and SS BRS in vitro were shown in Fig. 3. The drug burst release ratios of two groups were both lower than 5% within 1 day (marked by a dashed line in the figure). After the drug burst, the drug release displayed a linear relationship with time subsequently. The drug release rate constant calculated through y=kt was 0.74%/day for JDBM BRS and 0.34%/day for SS BRS respectively. It was obvious that the drug release rate of JDBM BRS was much higher than SS BRS.

3.3 Quantitative coronary angiographic results

As shown in Table 1, the reference vessel diameters were similar between the groups. Minimal luminal diameter behaved similarly pre-procedure and immediately after the procedure in both groups. Angiographic follow-up data were available in all experimental animals at 30, 90, and 180 days follow-up. The results showed that there was no significant difference in minimal luminal diameter between groups.

3.4 OCT Findings

OCT images in porcine coronary arteries implanted with JDBM BRS and Firehawk stent for 180 days were shown in Fig. 4. At the cross-section level, no significant difference of uncovered struts was found between the two groups, and there was no difference in thrombus occurrence between the two groups.

3.5 Micro-CT study

At 30 and 90 days post implantation, the JDBM BRS was harvested and examined using micro-CTto evaluate the stent degradation through time, as shown in Fig. 5. At 30 days, the stent still maintained good integrity, indicating that the stent could still provide radial support to the vascular wall. At 90 days, although some struts had transferred from the metal to degradation products, which displayed as light gray in the image, no macroscopic break in the stent struts was observed. This result suggested that the JDBM BRS could still provide radial support at 90 days post implantation.

3.6 SEM analysis

SEM analysis showed good expansion of all stents at 30 days. The majority of stent surfaces showed nearly complete coverage by endothelium in both groups. None of the groups showed obstructive luminal thrombi, which indicated that this novel JDBM BRS induced less inflammation within the vessel wall. Representative images are shown in Fig. 6.

3.7 Histomorphometry and histology

The in vivo safety and efficacy of JDBM BRS was evaluated by the histological analysis of stented arteries in porcine. All animals underwent successful implantation of JDBM BRS and Firehawk rapamycin-eluting stent. There was no signi difference in internal elastic membrane area, luminal area, neointimal thickness, neointimal area, and percent stenotic lumen among JDBMBRS and control groups, and injury and inflammation scores were similar in both groups, as shown in Table 2 and Fig. 7.

Discussion

Drug-eluting BRS was designed to overcome the limitations of DES such as a chronic local inflammatory reaction and late stent thrombosis in the treatment of CAD. Theoretically, ideal BRS

should have adequate radial support for a period of about 6 months to limit recoil and constrictive remodeling. They should have as low crossing profile as possible and be flexible enough to allow delivery in more challenging anatomical disease together with thin struts to limit the healing response. At last, they should be completely absorbed as soon as possible after its therapeutic period is over. Based on this theory, the first generation drug-eluting BRS was designed and had shown an efficacy profile comparable to DES in de novo native coronary artery lesions [24-29], indicating its long term advantages in the treatment of CAD.

BRS has thus been undergoing rapid development in recent years, and various types of polymers have been used. The most common polymer used is PLLA, which provides sufficient radial strength to the vessel. The radial strength is approximately 1200 mmHg directly after the implantation of the scaffold and it is as much as 800 mmHg after 1 year [9]. The degradation of PLLA occurs through hydrolysis of the ester bonds into small particles that are phagocytosed by macrophages with lactates generating. Lactates are subsequently converted into pyruvates and enter Kreb's cycle, where they are metabolized to CO_2 and H_2O [30]. Absorb bioresorbable vascular stent (BVS), the first PLLA based drug-eluting BRS, demonstrated no difference in MACE when compared with traditional DES after one-year clinical follow-up [25]. However, a further study demonstrated the poor safety results of it, which led to Abbott Vascular halt production of Absorb [31]. Several limitations of PLLA should be addressed. First of all, overexpansion of PLLA may result in strut fractures because of its limitation in expansion and optimal scaffold apposition. Plus, reasonable device deployment is different for PLLA scaffolds because of its lack of radiopacity. Moreover, the behavior of PLLA scaffolds is limited in complex lesions such as bifurcations, calcified, long or diffusely diseased lesions [32].

Another polymer used in BRS technology is tyrosine polycarbonate, with its resulting copolymer a biodegradable polyester carbonate called poly(lactic acid-co-L-tyrosine). Following absorption, water, carbon dioxide, ethanol and iodinated tyrosine are the end products and excreted from the body [33]. Recently, REVA Medical developed a proprietary, inherently radiopaque polymer composed of tyrosine analogs and other natural metabolites that allow visualization using conventional angiography. The clinical evidence of tyrosine polycarbonate polymer is promising but needs more research [34].

Mg is an essential element for several enzymes in the human body and Mg-based scaffolds have been widely investigated owing to its high mechanical strength. It is possible for Mg to form a scaffold with thinner struts, with its degradation products of inorganic salts [14, 35]. In comparison to PLLA, Mg shows better radial force, pushability and trackability [36]. Mg has been reported to have potential antithrombotic properties due to its electronegative charge during degradation [14, 35, 37, 38]. On the other hand, the reduction in ischemia-reperfusion injury using Mg was experimentally documented [39]. An Mg-mediated inhibition of the endothelin-1 production is also known, and prevents endothelin-induced vasoconstriction [40, 41]. In vitro tests of Mg based BRS showed a decreased smooth muscle cell proliferation and an increased endothelial cell proliferation [42]. However, most Mg alloys exhibit excessive corrosion rates with complete biodegradation within 3 months, which led to early vessel recoil and restenosis. This limits its clinical application, and the only reliable study available for Mg validation to date is BIOSOLVE II, where only 123 patients were treated and any kind of complex lesion was excluded.

JDBM is a new type of patented Mg–Nd–Zn-Zr based alloy to conquer the disadvantage of Mg,

and it has already been proved to exhibit good mechanical property and much slower degradation rate [15, 16]. In the present study, we first immerse JDBM in HF to form MgF_2 film for lower degradation of JDBM, and PDLLA/RAPA coating was prepared on these stents to further reduce the degradation rate and prevent restenosis of the blood vessels by controlled and efficient rapamycin release to the coronary artery.

To explore the biocompatibility and specific biological functions of this novel JDBM BRS, in vitro and in vivo characterizations were carried out. In vitro biological functions including effects on smooth muscle cells and drug release were studied. It is found that the proliferation of smooth muscle cells in different groups is similar after 1 day. However, after 3 days, in contrast to the significant increase in NC, the cell density of HF-JDBM group has no obvious change. This means cell proliferation was inhibited. When adding PDLLA coating on fluorinated JDBM, the cells in the PDLLA group propagate fast again. That is because the degradation rate of HF-JDBM is reduced by adding PDLLA coating, and the high concentration magnesium ions release was avoided which benefited cell proliferation [43]. When further adding rapamycin on PDLLA coating, the cell density decreases in the PDLLA/RAPA group. This is due to the inhabitation effects on smooth muscle cells of rapamycin release. Rapamycin release plays an important role in intimal hyperplasia inhibition and anti-thrombosis in drug eluting stents, so JDBM BRS and SS DES with the same structure and drug coating are used to evaluate the drug release. The burst drug release rate is low for both stents. After one day, the drug release rate of JDBM BRS is gradually higher than SS DES and shows a linear relationship with time. This is because the degradation of Mg alloys can accelerate the rapamycin release, which is beneficial for lower restenosis risks. After 60 days, about 50% of rapamycin has been released. In vitro study reveals the great potential

of JDBM BRS.

For in vivo evaluation, quantitative coronary angiographic, OCT, Micro-CT, SEM and histomorphometry were carried out. It is found that the vessel implanted with JDBM BRS and Firehawk can both have complete endothelialization after 30 days. And there is no distinct thrombosis, intimal hyperplasia, restenosis, and inflammation during the longer implanted time to 180 days for two kinds of stents. Moreover, JDBM BRS shows excellent structural integrity after being implanted for 90 days. This means it can afford enough support for more than three months. Compared with the JDBM bare stents implanted results that most of the corners and connecting rods are broken only after 1 month, adding PDLLA/RAPA coating can reduce the degradation of JDBM stents dramatically resulting in lower abnormal vasoconstriction risks and better vascular remodeling.

From in vitro and in vivo results mentioned above, we can conclude that after being loaded with PDLLA/RAPA coating, JDBM BRS can inhibit smooth muscle cell proliferation and prevent intimal hyperplasia and restenosis by controlling rapamycin release. At the same time, the degradation rate of JDBM stents is greatly reduced by PDLLA coating that can meet safe enough support for vessels. Therefore, JDBM BRS is a promising candidate for the treatment of coronary artery disease.

Conclusions

JDBM alloy based rapamycin-eluting BRS could inhibit the proliferation of smooth muscle cells and prevent restenosis of the blood vessels by controllable and efficient rapamycin release, and exhibited moderate degradation rate, which maintained general integrity at 3 months post implantation. These results demonstrate that JDBM based rapamycin-eluting BRS has great

potential as an alternative to the present DES for the treatment of coronary artery disease.

Competing interests

The authors declare that they have no competing interests.

Acknowledgements

This research was supported by grants from the National Natural Science Foundation of China (No. U1804251), the Science and Technology Commission of Shanghai Municipality, China (No. 14DZ1940803) and medical-engineering cross fund of Shanghai Jiao Tong University, China (YG2019ZDA02). The funding source had no input into the design or conduct of the study and had no control over the published results.

Authors' contributions

CXC performed scaffold design and preparation. YJS, JP performed coating preparation and in vitro experiments. ZBZ and DPD performed the angiography procedure and OCT study. JZZ, XYZ, JLN analyzed all experimental data and wrote the manuscript. The molecular studies were performed by JZZ. GYY and RYZ designed this study and observed the whole study process. JZZ, XYZ, and JLN contributed equally. All authors read and approved the final version of the manuscript.

References

[1] Iqbal J, et al. Comparison of zotarolimus- and everolimus-eluting coronary stents: final 5-year report of the RESOLUTE all-comers trial. Circulation Cardiovascular interventions. 8, e002230 (2015).

[2] Sousa-Uva M, et al. 2018 ESC/EACTS Guidelines on myocardial revascularization. European journal of cardio-thoracic surgery : official journal of the European Association for Cardio-thoracic Surgery. 55, 4-90 (2019).

[3] Finn AV, et al. Pathological correlates of late drug-eluting stent thrombosis: strut coverage as a marker of endothelialization. Circulation. 115, 2435-2441 (2007).

[4] Cook S, et al. Correlation of intravascular ultrasound findings with histopathological analysis of thrombus aspirates in patients with very late drug-eluting stent thrombosis. Circulation. 120, 391-399 (2009).

[5] Joner M, et al. Pathology of drug-eluting stents in humans: delayed healing and late thrombotic risk. Journal of the American College of Cardiology. 48, 193-202 (2006).

[6] Virmani R, et al. Localized hypersensitivity and late coronary thrombosis secondary to a sirolimus-eluting stent: should we be cautious? Circulation. 109, 701-705 (2004).

[7] Daemen J, et al. Early and late coronary stent thrombosis of sirolimus-eluting and paclitaxel-eluting stents in routine clinical practice: data from a large two-institutional cohort study. Lancet. 369, 667-678 (2007).

[8] Wenaweser P, et al. Incidence and correlates of drug-eluting stent thrombosis in routine clinical practice. 4-year results from a large 2-institutional cohort study. Journal of the American College of Cardiology. 52, 1134-1140 (2008).

[9] Wiebe J, et al. Current status of bioresorbable scaffolds in the treatment of coronary artery disease. Journal of the American College of Cardiology. 64, 2541-2551 (2014).

[10] Iqbal J, et al. Bioresorbable scaffolds: rationale, current status, challenges, and future. European heart journal. 35, 765-776 (2014).

[11] Onuma Y, et al. Bioresorbable scaffold: the advent of a new era in percutaneous coronary and peripheral revascularization? Circulation. 123, 779-797 (2011).

[12] Ormiston JA, et al. First-in-human implantation of a fully bioabsorbable drug-eluting stent: the

BVS poly-L-lactic acid everolimus-eluting coronary stent. Catheterization and cardiovascular interventions : official journal of the Society for Cardiac Angiography & Interventions. 69, 128-131 (2007).

[13] Serruys PW, et al. From metallic cages to transient bioresorbable scaffolds: change in paradigm of coronary revascularization in the upcoming decade? European heart journal. 33, 16-25b (2012).

[14] Heublein B, et al. Biocorrosion of magnesium alloys: a new principle in cardiovascular implant technology? Heart. 89, 651-656 (2003).

[15] Zhang X, et al. Microstructure, mechanical properties, biocorrosion behavior, and cytotoxicity of as-extruded Mg-Nd-Zn-Zr alloy with different extrusion ratios. Journal of the mechanical behavior of biomedical materials. 9, 153-162 (2012).

[16] Mao L, et al. Nanophasic biodegradation enhances the durability and biocompatibility of magnesium alloys for the next-generation vascular stents. Nanoscale. 5, 9517-9522 (2013).

[17] Feyerabend F, et al. Evaluation of short-term effects of rare earth and other elements used in magnesium alloys on primary cells and cell lines. Acta biomaterialia. 6, 1834-1842 (2010).

[18] Zhang X, et al. Effects of extrusion and heat treatment on the mechanical properties and biocorrosion behaviors of a Mg-Nd-Zn-Zr alloy. Journal of the mechanical behavior of biomedical materials. 7, 77-86 (2012).

[19] Mao L, et al. Nanophasic biodegradation enhances the durability and biocompatibility of magnesium alloys for the next-generation vascular stents. Nanoscale. 5, 9517-9522 (2013).

[20] Shi Y, et al. Understanding the effect of magnesium degradation on drug release and anti-proliferation on smooth muscle cells for magnesium-based drug eluting stents. Corrosion ence. 123, 297-309 (2017).

[21] Liu F, et al. The processing of Mg alloy micro-tubes for biodegradable vascular stents. Materials ence & Engineering C. 48, 400-407 (2015).

[22] In vitro and in vivo degradation of rapamycin-eluting Mg-Nd-Zn-Zr alloy stents in porcine coronary arteries. Mater Eng C Mater Biol Appl. 80, 1-6 (2017).

[23] Zhu JZ, et al. Hemocompatibility of drug-eluting coronary stents coated with sulfonated poly (styrene-block-isobutylene-block-styrene). Biomaterials. 33, 8204-8212 (2012).

[24] Verheye S, et al. A next-generation bioresorbable coronary scaffold system: from bench to first clinical evaluation: 6- and 12-month clinical and multimodality imaging results. JACC Cardiovascular interventions. 7, 89-99 (2014).

[25] Abizaid A, et al. The ABSORB EXTEND study: preliminary report of the twelve-month clinical outcomes in the first 512 patients enrolled. EuroIntervention : journal of EuroPCR in collaboration with the Working Group on Interventional Cardiology of the European Society of Cardiology. 10, 1396-1401 (2015).

[26] Ellis SG, et al. Everolimus-Eluting Bioresorbable Scaffolds for Coronary Artery Disease. The New England journal of medicine. 373, 1905-1915 (2015).

[27] Serruys PW, et al. A bioresorbable everolimus-eluting scaffold versus a metallic everolimus-eluting stent for ischaemic heart disease caused by de-novo native coronary artery lesions (ABSORB II): an interim 1-year analysis of clinical and procedural secondary outcomes from a randomised controlled trial. Lancet. 385, 43-54 (2015).

[28] Abizaid A, et al. Serial Multimodality Imaging and 2-Year Clinical Outcomes of the Novel DESolve Novolimus-Eluting Bioresorbable Coronary Scaffold System for the Treatment of Single De Novo Coronary Lesions. JACC Cardiovascular interventions. 9, 565-574 (2016).

[29] Haude M, et al. Safety and performance of the second-generation drug-eluting absorbable metal scaffold in patients with de-novo coronary artery lesions (BIOSOLVE-II): 6 month results of a prospective, multicentre, non-randomised, first-in-man trial. Lancet. 387, 31-39 (2016).

[30] Ormiston JA, et al. A bioabsorbable everolimus-eluting coronary stent system for patients with single de-novo coronary artery lesions (ABSORB): a prospective open-label trial. Lancet. 371, 899-907 (2008).

[31] Puricel S, et al. Bioresorbable Coronary Scaffold Thrombosis: Multicenter Comprehensive Analysis of Clinical Presentation, Mechanisms, and Predictors. Journal of the American College of Cardiology. 67, 921-931 (2016).

[32] Kitabata H, et al. Bioresorbable metal scaffold for cardiovascular application: current knowledge and future perspectives. Cardiovascular revascularization medicine : including molecular interventions. 15, 109-116 (2014).

[33] Gomez-Lara J, et al. Angiographic geometric changes of the lumen arterial wall after bioresorbable vascular scaffolds and metallic platform stents at 1-year follow-up. JACC Cardiovascular interventions. 4, 789-799 (2011).

[34] Abizaid A, et al. 6-Month Clinical and Angiographic Outcomes of a Novel Radiopaque Sirolimus-Eluting Bioresorbable Vascular Scaffold: The FANTOM II Study. JACC Cardiovascular interventions. 10, 1832-1838 (2017).

[35] Waksman R, et al. Safety and efficacy of bioabsorbable magnesium alloy stents in porcine coronary arteries. Catheterization and cardiovascular interventions : official journal of the Society for Cardiac Angiography & Interventions. 68, 607-617; discussion 618-609 (2006).

[36] Smith LF, et al. Intravenous infusion of magnesium sulphate after acute myocardial infarction:

effects on arrhythmias and mortality. International journal of cardiology. 12, 175-183 (1986).

[37] Rukshin V, et al. Intravenous magnesium in experimental stent thrombosis in swine. Arteriosclerosis, thrombosis, and vascular biology. 21, 1544-1549 (2001).

[38] Rukshin V, et al. Comparative antithrombotic effects of magnesium sulfate and the platelet glycoprotein IIb/IIIa inhibitors tirofiban and eptifibatide in a canine model of stent thrombosis. Circulation. 105, 1970-1975 (2002).

[39] Christensen CW, et al. Magnesium sulfate reduces myocardial infarct size when administered before but not after coronary reperfusion in a canine model. Circulation. 92, 2617-2621 (1995).

[40] Kemp PA, et al. Assessment of the effects of endothelin-1 and magnesium sulphate on regional blood flows in conscious rats, by the coloured microsphere reference technique. British journal of pharmacology. 126, 621-626 (1999).

[41] Berthon N, et al. Effect of magnesium on mRNA expression and production of endothelin-1 in DOCA-salt hypertensive rats. Journal of cardiovascular pharmacology. 42, 24-31 (2003).

[42] Sternberg K, et al. Magnesium used in bioabsorbable stents controls smooth muscle cell proliferation and stimulates endothelial cells in vitro. Journal of biomedical materials research Part B, Applied biomaterials. 100, 41-50 (2012).

[43] Zheng YF, et al. Biodegradable metals. Materials Science & Engineering, R Reports: A Review Journal. (2014).

Figure legends

Figure 1 The adhesion morphologies of A7r5 cells on HF-JDBM, PDLLA coated JDBM, PDLLA/RAPA coated JDBM, and negative control (NC) for 1 and 3 days (Stained with Calcein-AM, and green signals represent live cells).

Figure 2 Statistics of A7r5 cell densities on various samples (Five fields are counted for each group and the results are presented as mean ± S.D.).

Figure 3 Drug release kinetic profiles of JDBM BRS and SS BRS.

Figure 4 Representative OCT images of JDBM BRS and Firehawk stent in the porcine coronary artery at day 180 after stent implantation.

Figure 5 Micro-CT result of residual JDBM BRS at 30 and 90 days post implantation.

Figure 6 SEM images of JDBM BRS vs. Firehawk in the porcine coronary artery at 30 days post implantation.

Figure 7 Representative histological images of JDBM BRS and Firehawk groups after implanted into porcine arteries for 30, 90, and 180 days. Sections are stained with Masson.

Table 1 Minimal lumen diameter of stented coronary artery segments measured by quantitative coronary angiographic (QCA)

	Firehawk	JDBM BRS	P Value
Pre-procedure, n	4	4	
Reference vessel diameter, mm	2.63 ± 0.04	2.61 ± 0.05	0.6523
Minimal luminal diameter, mm	2.60 ± 0.08	2.56 ± 0.07	0.6443
30 day follow-up, n	4	4	
Minimal lumen diameter, mm	2.49 ± 0.13	2.40 ± 0.15	0.4577
90 day follow-up, n	4	4	
Minimal lumen diameter, mm	2.33 ± 0.15	2.18 ± 0.23	0.3455
180 day follow-up, n	4	4	
Minimal lumen diameter, mm	2.13 ± 0.11	2.01 ± 0.25	0.2165

Values are expressed as mean ± SD. n: number of stented arterial segments.

Table 2 Morphometry comparisons

	Firehawk	JDBM BRS	*P* Value
30 day follow-up, n	4	4	
Injury score	1.53±0.11	1.57±0.14	0.6776
Mean LA, mm^2	4.56±0.45	4.46±0.63	0.6567
Mean IEM, mm^2	5.67±0.57	5.74±0.77	0.5456
Mean NA, mm^2	1.13±0.44	1.35±0.76	0.4477
Mean NT, mm	0.31±0.09	0.45±0.11	0.4876
Percent area stenosis, %	0.09±0.02	0.13±0.07	0.3676
Inflammation score	1.02±0.14	1.15±0.28	0.3577
90 day follow-up, n	4	4	
Injury score	2.04±0.32	2.37±0.44	0.6356
Mean LA, mm^2	3.96±0.45	3.75±0.73	0.4567
Mean IEM, mm^2	5.99±0.88	5.84±0.77	0.6657
Mean NA, mm^2	1.96±0.95	2.08±1.11	0.3234
Mean NT, mm	0.51±0.15	0.70±0.23	0.3823
Percent area stenosis, %	0.15±0.05	0.20±0.08	0.3467
Inflammation score	0.89±0.15	1.07±0.28	0.2122
180 day follow-up, n	4	4	
Injury score	2.13±0.31	2.39±0.54	0.6745
Mean LA, mm^2	3.66±0.77	3.36±0.73	0.3562
Mean IEM, mm^2	6.38±1.14	6.26±1.57	0.3245

Mean NA, mm^2	2.66±0.83	2.86±1.16	0.3649
Mean NT, mm	0.73±0.21	0.92±0.35	0.2556
Percent area stenosis, %	0.24±0.05	0.29±0.12	0.2345
Inflammation score	0.67±0.23	0.87±0.38	0.2187

LA: average lumen area; IEM: average internal elastic membrane area; NA: average neointimal area; NT: average neointimal thickness; n: number of sections.

Figure 1

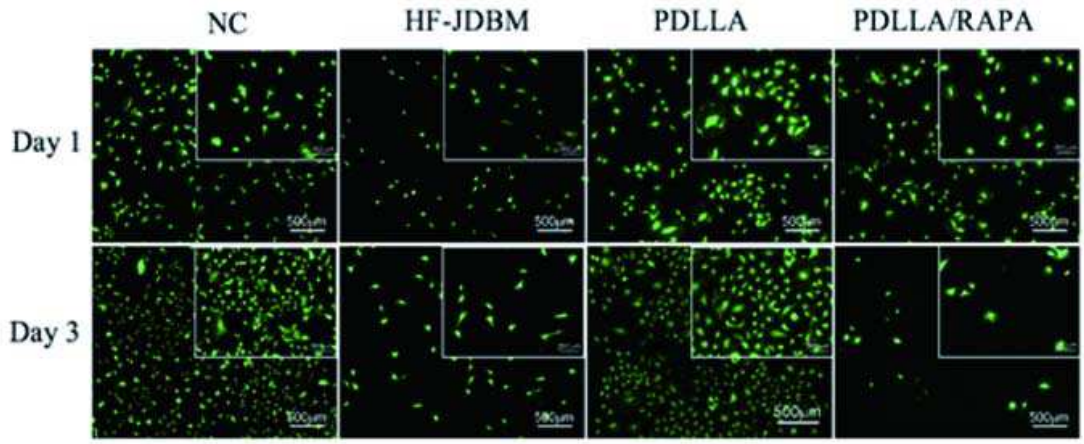

Figure 2

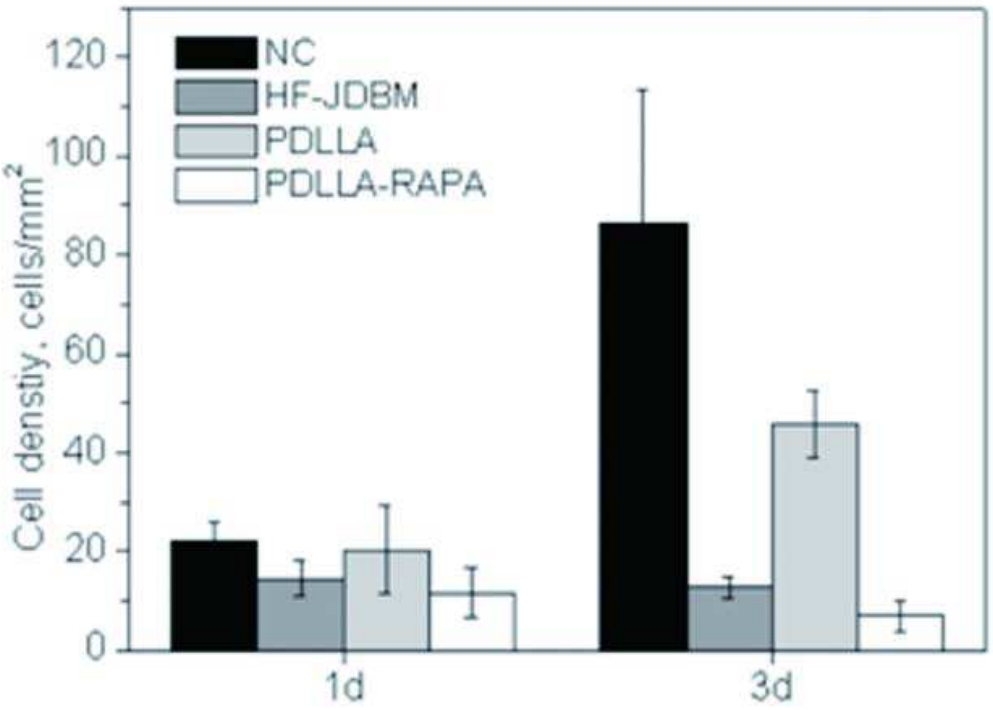
NC
HF-JDBM
PDLLA
PDLLA-RAPA
Cell denstiy, cells/mm²
120
100
80
60
40
20
0
1d
3d

Figure 3

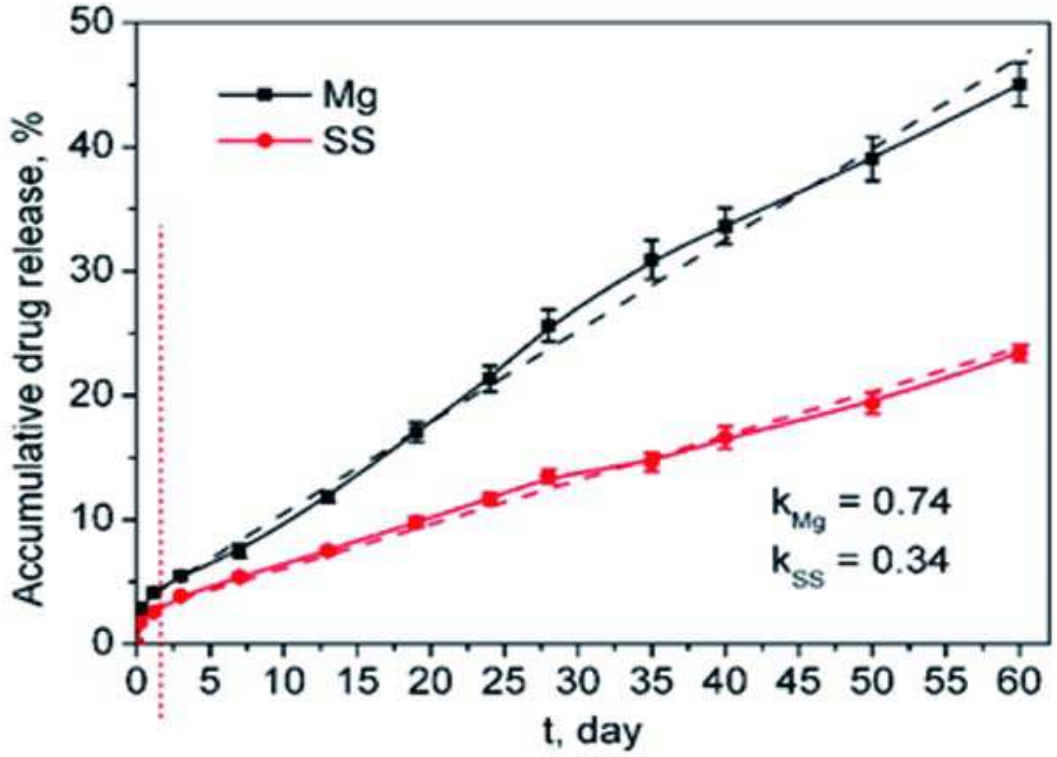
Mg
SS
Accumulative drug release, %
t, day
k_{Mg} = 0.74
k_{SS} = 0.34
0
10
20
30
40
50
0
5
10
15
20
25
30
35
40
45
50
55
60

Figure 4

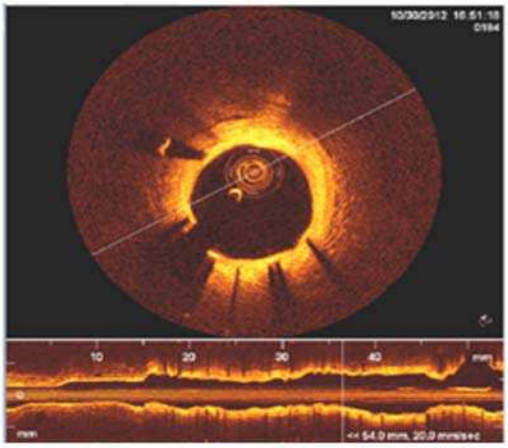

Firehawk

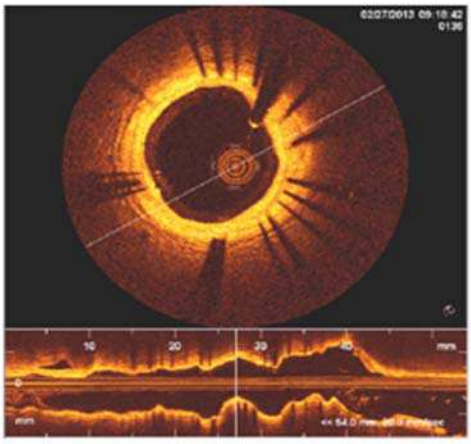

JDBM-MgF2 BRS

Figure 5

day 30 day 90

Figure 6

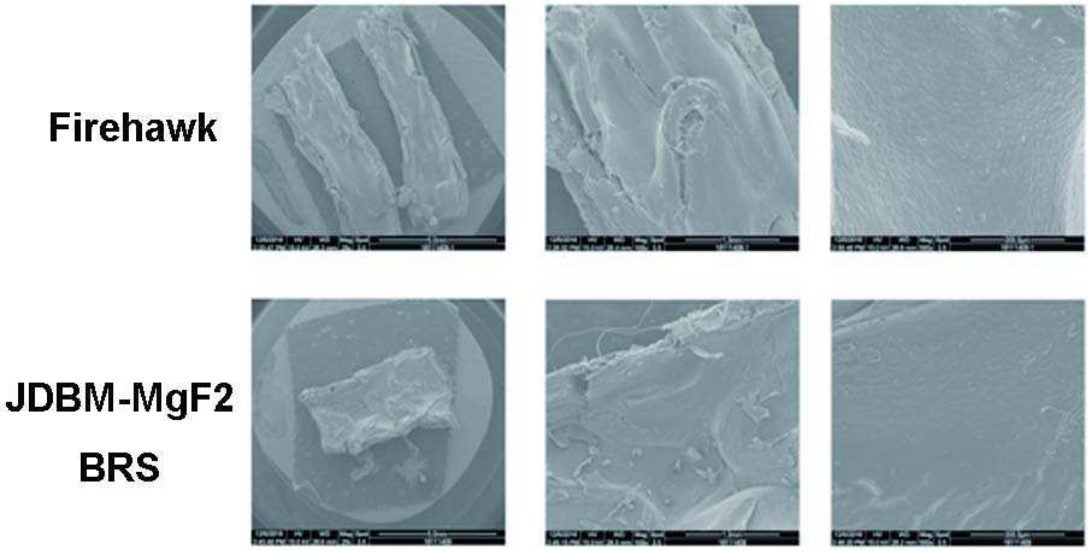

Figure 7

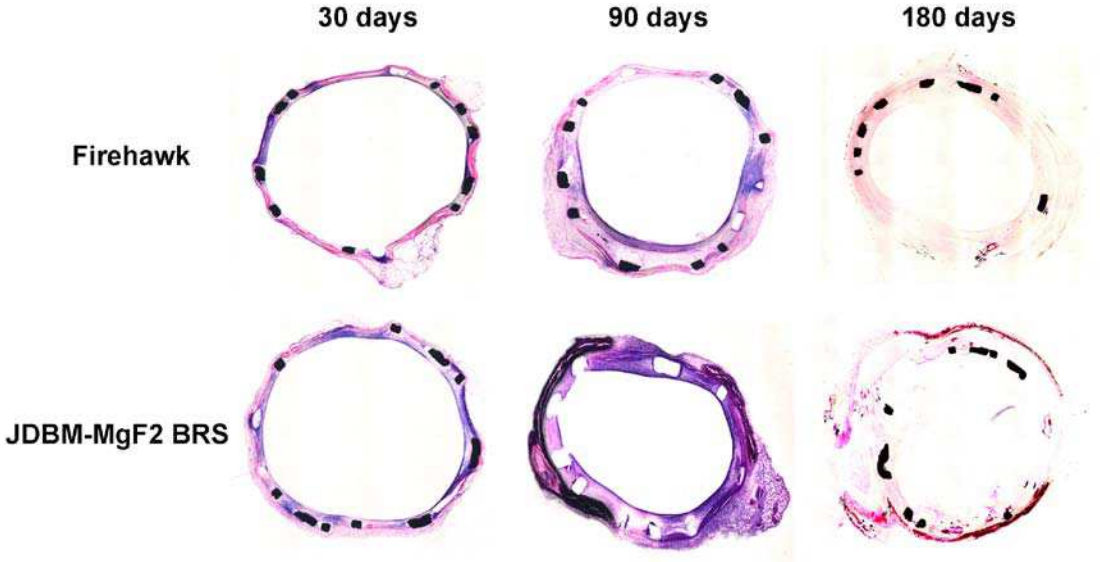

Figures

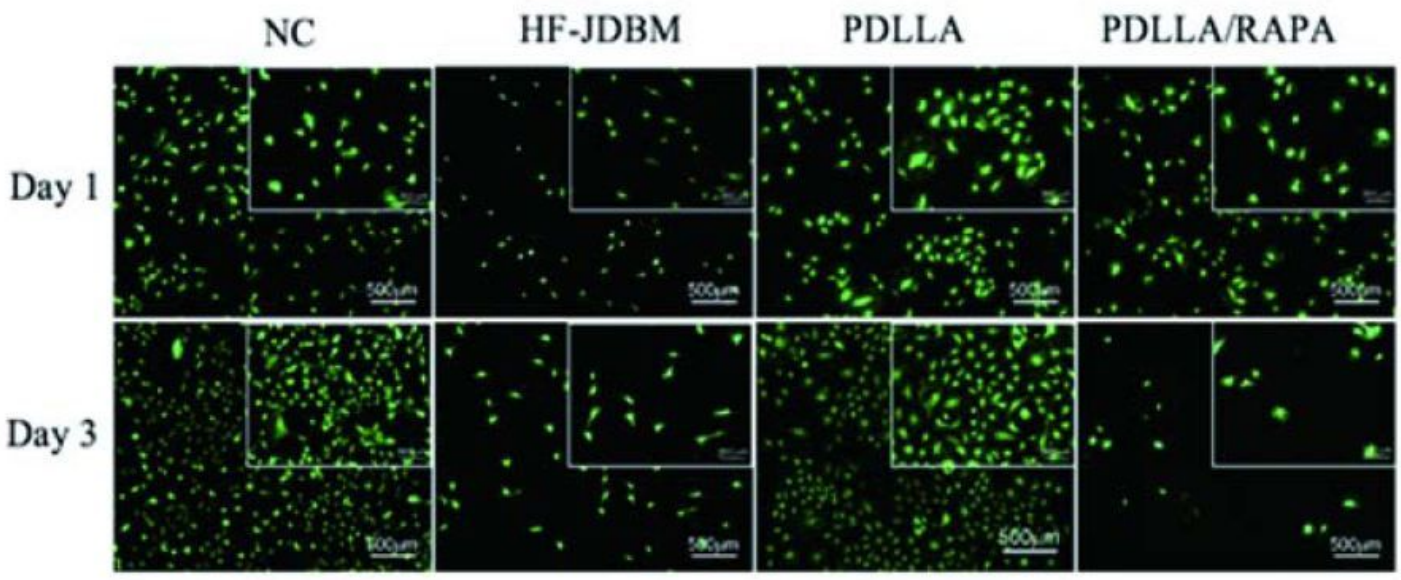

Figure 1

The adhesion morphologies of A7r5 cells on HF-JDBM, PDLLA coated JDBM, PDLLA/RAPA coated JDBM, and negative control (NC) for 1 and 3 days (Stained with Calcein-AM, and green signals represent live cells).

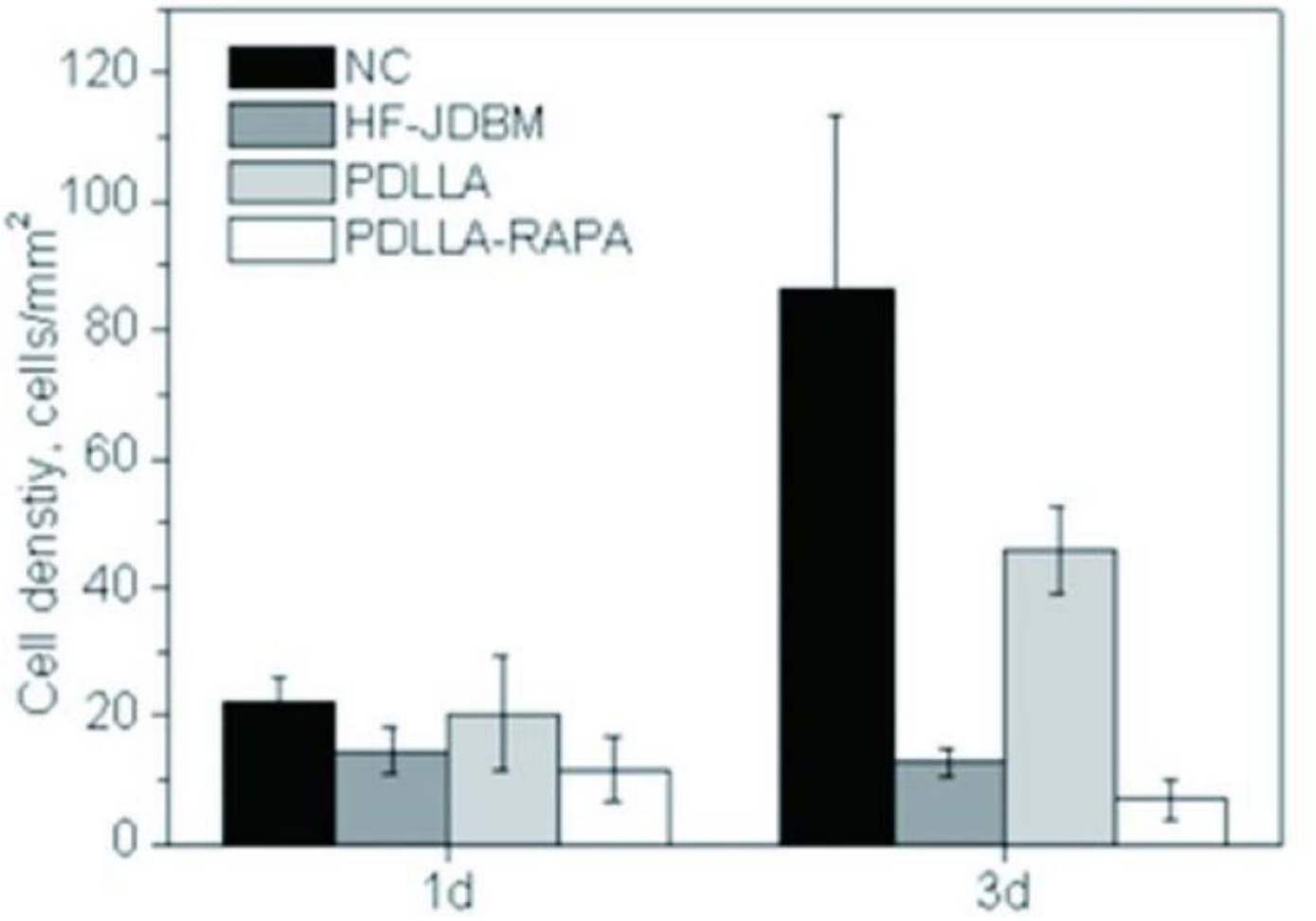

Figure 2

Statistics of A7r5 cell densities on various samples (Five fields are counted for each group and the results are presented as mean ± S.D.).

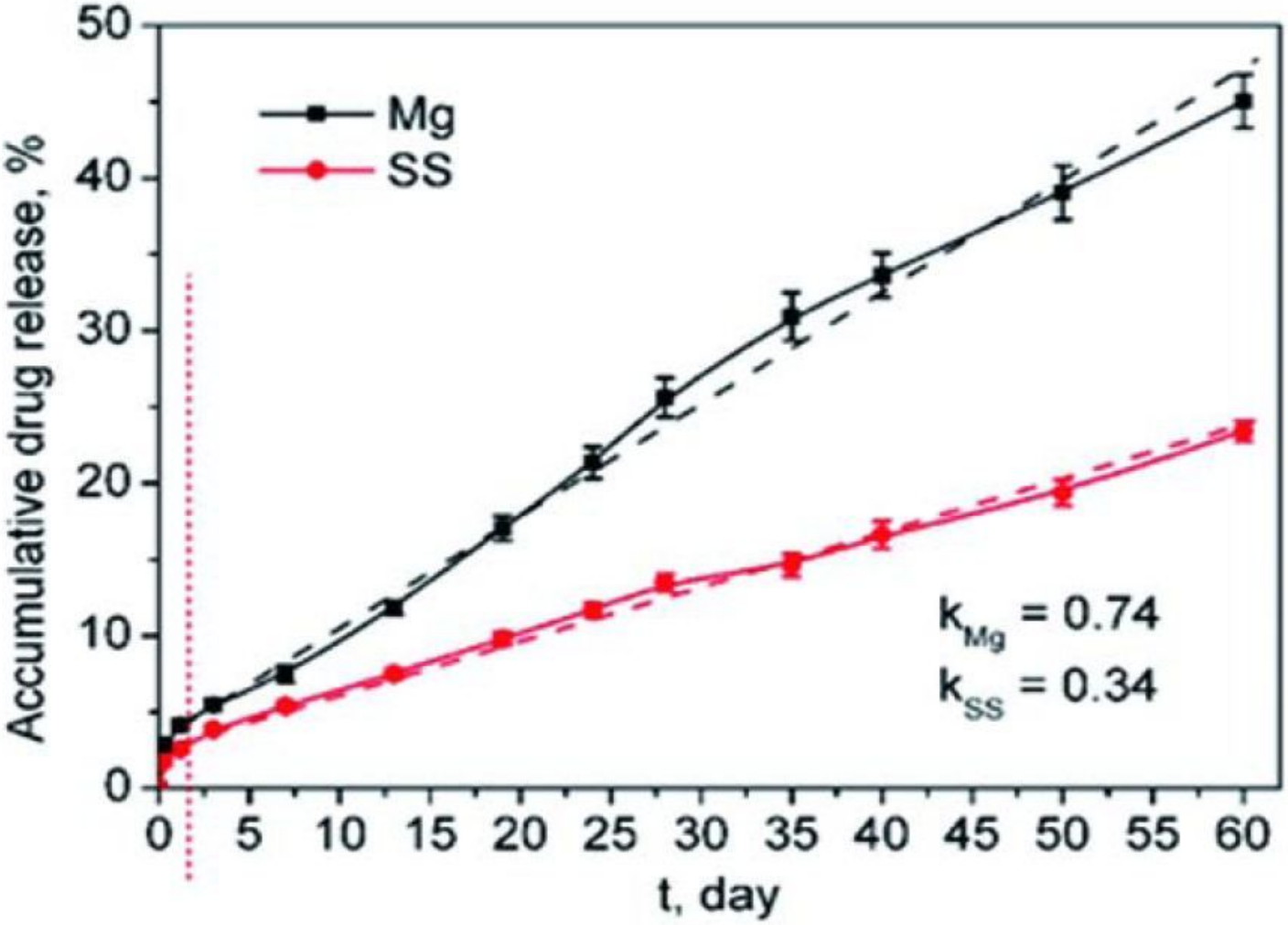

Figure 3

Drug release kinetic profiles of JDBM BRS and SS BRS.

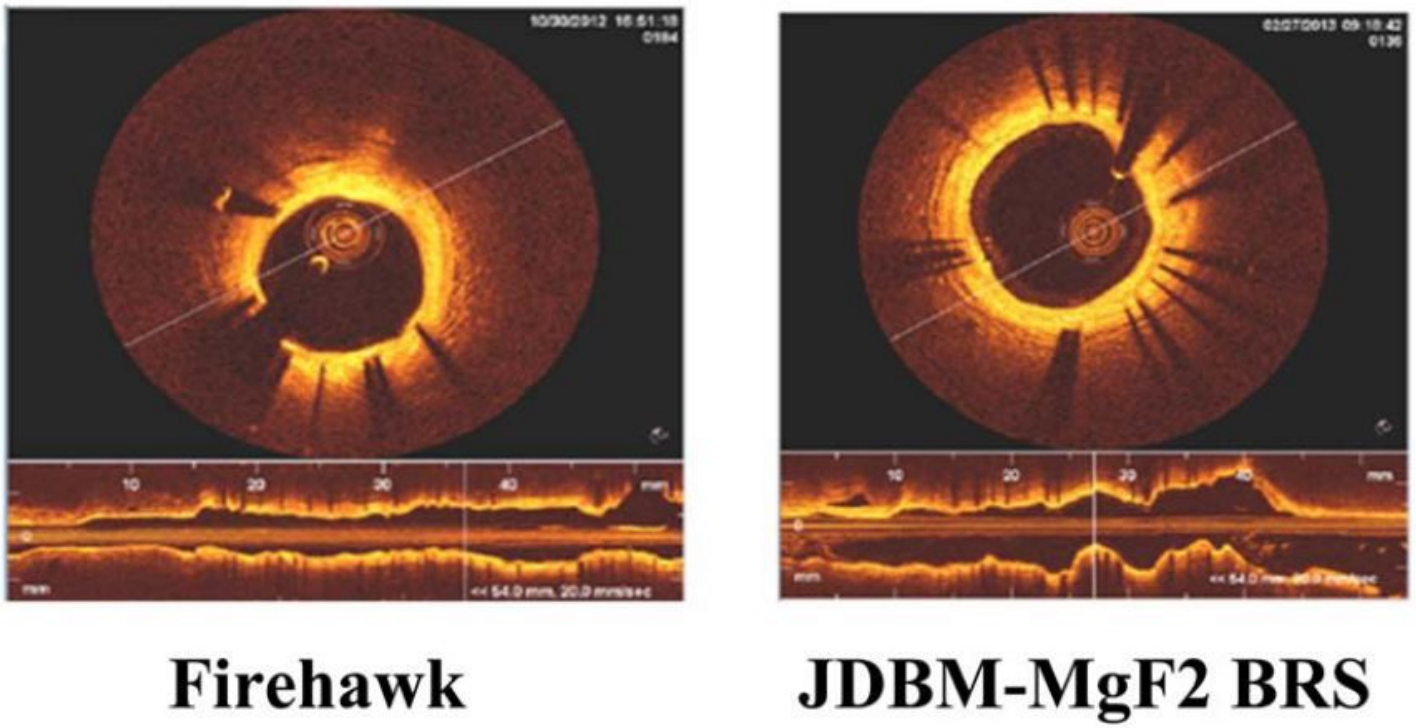

Figure 4

Representative OCT images of JDBM BRS and Firehawk stent in the porcine coronary artery at day 180 after stent implantation.

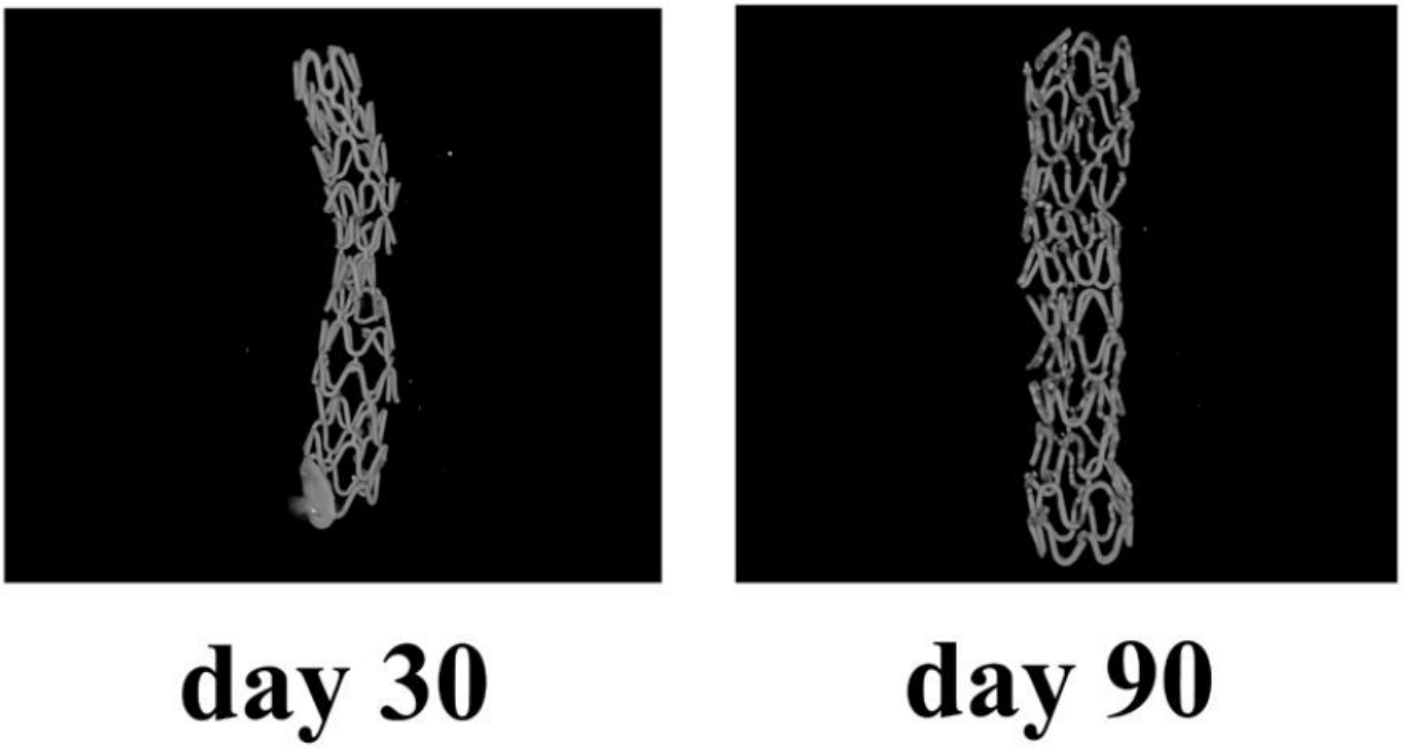

Figure 5

Micro-CT result of residual JDBM BRS at 30 and 90 days post implantation.

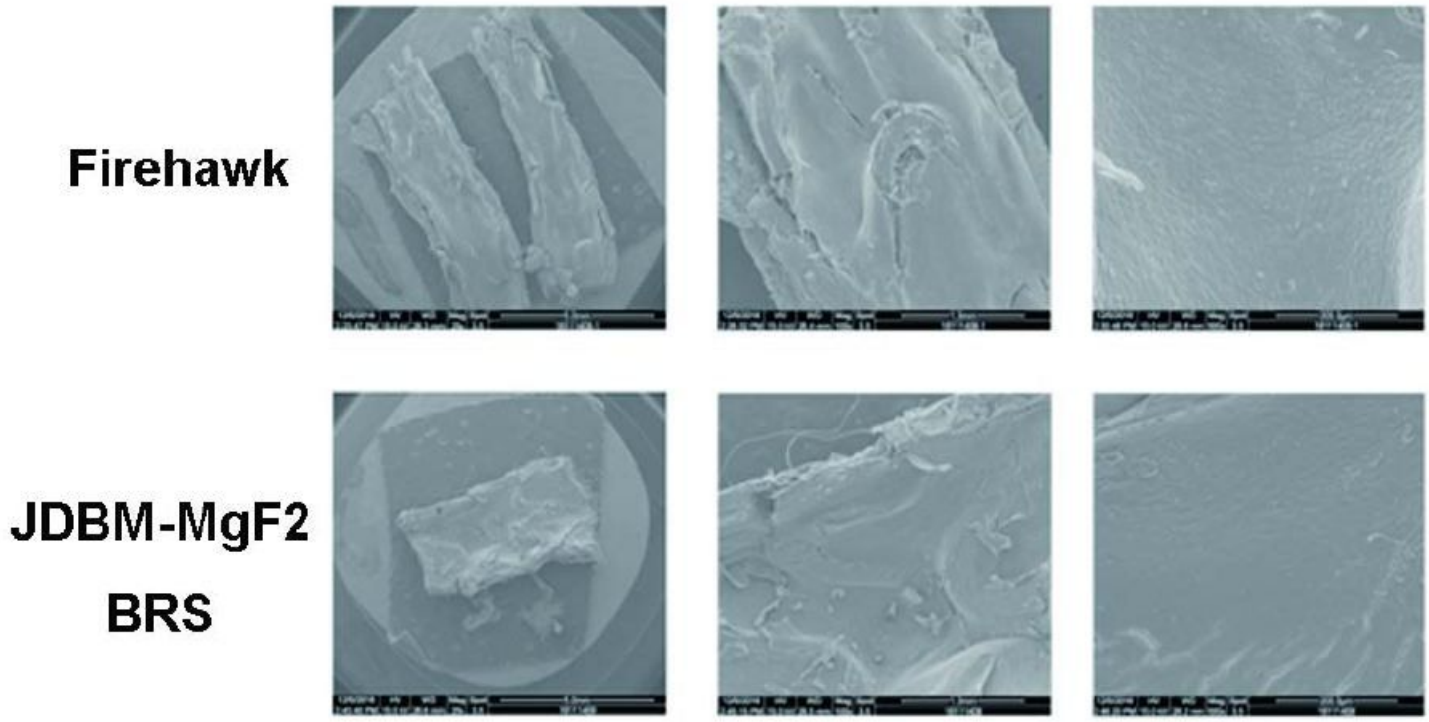

Figure 6

SEM images of JDBM BRS vs. Firehawk in the porcine coronary artery at 30 days post implantation.

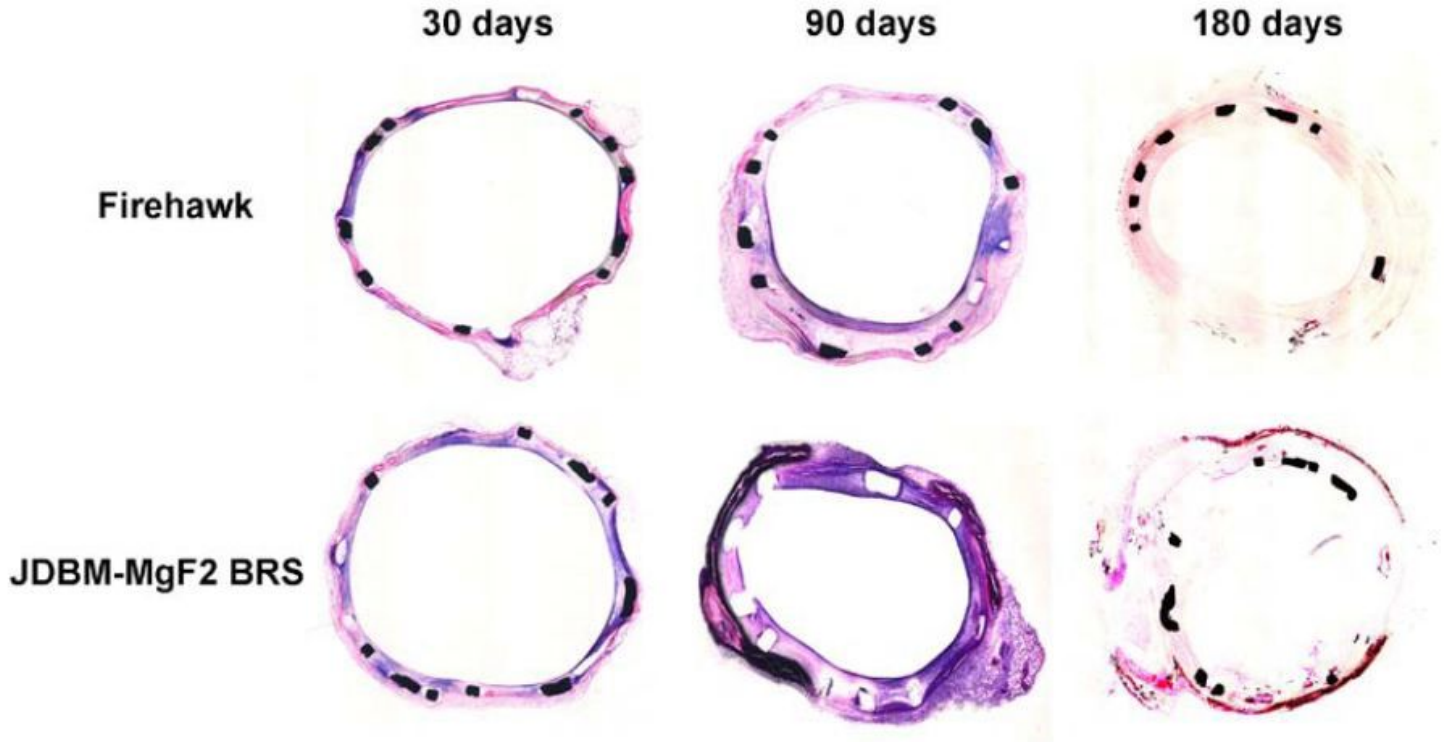

Figure 7

Representative histological images of JDBM BRS and Firehawk groups after implanted into porcine arteries for 30, 90, and 180 days. Sections are stained with Masson.